

# Eggshell Membrane Assisted CdS Nanoparticles for Manganese Removal in Water Treatment

Anurag Roy\*, Sasireka Velusamy, Tapas K. Mallick and Senthilarasu Sundaram\*

Environment and Sustainability Institute, University of Exeter, Penryn Campus, Cornwall TR10 9FE, U.K.

\*Corresponding author: E-mail: A.Roy30@exeter.ac.uk (A.R.); S.Sundaram@exeter.ac.uk (S.S.); Tel: 01326 259486

DOI: 10.5185/amlett.2021.031609

Domestic food waste chicken eggshells can produce naturally abundant protein-based eggshell membranes (ESMs), which is used as a less-explored source of sulphur to synthesize hexagonal CdS nanoparticles (NPs) under 365 nm (UVA) light irradiation. The perspective of CdS NPs synthesis in the way of UVA light irradiation soakage technique using ESM is distinctive compare to other traditional methods. Various physicochemical methods were employed to validate the formation of CdS NP using ESM assisted process. The obtained NPs exhibit an average particle size of ~5 nm as obtained from the transmission electron microscopy study. The capability of the synthesized CdS NPs was further explored in the catalysis reaction for the decomposition of  $\text{KMnO}_4$ , considered as toxic  $\text{Mn}^{\text{VII}}$  (violet) ion source at room temperature. The degradation results as monitored by UV-Vis spectrophotometry analysis confirms the CdS NPs exhibit excellent catalytic activity towards the reduction of  $\text{KMnO}_4$ , toxic  $\text{Mn}^{\text{VII}}$  (violet) ion to  $\text{MnO}_2$  as non-toxic  $\text{Mn}^{\text{IV}}$  (brownish yellow) ion in aqueous solution (pH 7.0) at room temperature by 50 min. The  $\text{KMnO}_4$  decomposition reaction follows a pseudo-first-order reaction having the rate constant value of  $1.9 \times 10^{-2} \text{ min}^{-1}$ . This study encourages the potential use of natural waste materials for wastewater treatment.

## Introduction

Colloidal nanocrystals are mesoscopic materials filling up the region between the atomistic and the macroscopic worlds. The unique electronic, optical, and catalytic properties of metal and semiconductor nanoparticles (NPs), along with the different methods available for their preparation of controlled shape and size, offer exciting building blocks for nanoscale assemblies, structures and devices [1,2]. In recent years, there have been tremendous developments in the synthetic control of nanocrystal size, shape and composition, thus allowing the tailoring of their properties [3]. Several routes have been developed for the synthesis of semiconductor NPs with different shapes and sizes using different methods such as colloidal, sol-gel, co-precipitation, hydrothermal, micro-emulsion, sonochemical and template-based synthesis [4-6]. The most widely used synthetic technique for NPs is a colloidal technique, which gives uniform, monodisperse NPs with immense control over size, shape and composition of NPs. Despite that, a template acts as a scaffold. It controls the nucleation and growth of the stable particles, leading to the formation of nanostructure with control size, unique surface chemistry within it and with a morphology complementary to that of the template. Some hard templates include a porous membrane, polymer matrix, thin-film etc. [7,8]. Apart from these hard templates, soft templates have also been used in the synthesis of NPs. Metal NPs with controllable size, shape and distribution have advanced by small organic ligands, DNA, protein, peptide, dendritic architectures, organic molecular cages or polymers as

templates [9-12]. *In-situ* nucleation and growth of NPs can be achieved by using these soft templates. Besides, chicken eggshell membrane (ESM) has also emerged as a cost-effective bio-template for the synthesis of metal NPs [13-15]. ESM has a three dimensional-entangled structure of highly cross-linked fibres and porous site. The superabundant, economically benign character and unique features make ESM superior to other naturally available proteins like bovine serum albumin, human serum albumin etc. The ESM mainly consists of glycoproteins like collagen and several other amino acids glycine, cysteine, uronic acid etc. [16-18]. On the other hand, the presence of amino acids makes ESM a suitable platform to form stable metal NPs immobilized ESM. Over the last few years, ESM has been used as a soft template for the synthesis of Au, Ag and AuAg clusters in a cost-effective manner [19-21]. Besides, Su et al. (2011) prepared hierarchical ZnO single crystals by introducing ESM, which could grow at three dimensions into polyhedral single crystals through a surface sol-gel process followed by a calcination treatment [22].

Among II-VI, chalcogenides, CdS is an essential semiconductor with a direct bandgap of 2.42 eV [18,23]. CdS excels as a most promising photocatalyst with better properties like bandgap, good optical transmittance, and appropriate band potentials under different thermodynamic conditions for photocatalytic redox reactions. Generally, the synthesis of CdS employed through precipitation, hydrothermal, solid-state, chemical bath deposition, mechanical alloying, and pyrolysis of single-source precursor, which required high temperature with the use of

toxic and highly sensitive compounds. Therefore, it is of great significance to introduce effective synthesis pathways at low temperature, low cost, fast with well-controlled size and shape for desired applications [24,25]. CdS exists in three phases, including the wurtzite structure with a direct bandgap of ~2.4 eV, the zinc-blende structure with a bandgap of 2.55 eV and a high-pressure rocksalt structure with an indirect bandgap of ~1.5 eV. To maintain excellent optoelectronic properties, CdS must remain in the wurtzite structure for practical applications [26]. Therefore, the structural phase transformation in CdS crystals becomes an important issue, and it has attracted many theoretical and experimental studies.

Manganese (Mn) is one of the vital poisonous hazardous substances from water, causing significant environmental challenges. The excessive use of Mn containing products, mine waters, steel manufacturing industries discharged to nearby environment inevitably and led to environmental pollution. The oxidation state of Mn appears to be a key determinant of its distribution, accumulation and excretion. Manganese can exist in eleven oxidation states, which commonly occurring oxidation states are Mn<sup>II</sup>, Mn<sup>IV</sup> and Mn<sup>VII</sup>. These states are noxious, which generates a massive impact on the environment when it exceeds the permissible limits, moreover anthropogenic activities are the significant responsible role for the manganese contamination in our water resources [27-29]. Deficiency of manganese results in a wide variety of structural and physiological defects, including reduced growth rate, skeletal abnormalities, impaired reproduction, and unacceptable intake of manganese leads to severe health complications as well. There are different treatment methods available for degradation of heptavalent manganese, which are precipitation methods, oxidation, filtration, ion exchange, coagulation/flocculation, membrane filtration, electrochemical methods, biological treatment and adsorption [30-32]. Photocatalytic degradation technique has been considered as a promising technology for heavy metal removal compared to other methods, in this process it utilizes sunlight or indoor illumination lights; furthermore, photocatalysis is the most economical method and high-efficiency environmental protection method even though it has some limitations [33, 34]. The aim of this study lies in the synthesis of CdS NPs using ESM applying UVA light irradiation method and further application as an emerging redox catalyst for toxic Mn<sup>VII</sup> ion removal from aqueous solution. This approach can pave the way for the purification of acid manganese mine for the development of cleaner environment aspect.

## Experimental

### Materials

Cadmium acetate dihydrate (Sigma Aldrich), acetic acid (Merck) and potassium permanganate (Merck) are used without further purification for the experiment. Material characterization is illustrated in the Supplementary Information (SI).

### Synthesis of ESM assisted CdS

The cleaned eggshells (ESs) were treated with dilute acetic acid (50% diluted with water) to extract the membrane (ESM) from the ES by soaking them for 8 hours. Once the calcium carbonate shell gets dissolved, the membranes were carefully collected and thoroughly washed with deionized water and then dried in air at room temperature. An ES consists of two significant parts such as the hard shell, which is made mainly of calcium carbonate; and the thin membrane that lines the inside of the hard shell. The membrane is made of protein fibres that contain a considerable amount of sulphur and carbon. Thus, this kind of bio-waste can be implied as a potential source of sulphur to synthesize CdS for this case. At the same time, ESM provides as a bio-inspired templating approach based on the control of nucleation and gestation of CdS formation. The extracted dried white ESM (0.2 gm) was added to an aqueous solution of 10 ml of cadmium acetate in the presence of an 8W UV (ultraviolet) lamp (UVLS-28 EL Series) having an average light intensity of 0.6 mW.cm<sup>-2</sup>, excited at 365 nm (3.39 eV) for 2 hours inside a UV-chamber. The white ESM changes its colour to orangish-yellow, which indicates the formation of the CdS that immobilized on the surface of ESM. Finally, an orangish-yellow part from the ESM has been collected through rapid washing with ethanol and water, respectively. The collected product then further calcined at 300°C for 1 hour, to eliminate any hydroxyl, carbonaceous materials and considered for further study. The overall synthesis process perceives a “greener” synthesis approach to develop nanomaterial synthesis [35,36]. By the soakage technique, the cadmium precursor ions were impregnated to the ESM fibres to form Cd-ESM hybrids. These Cd-ESM hybrids accordingly react with the labile sulphur ions associated with the ESM protein under a constant UV light irradiation to form CdS. In the interfacial soaking process, the large anionic groups (carboxylic, hydroxy, and amino residues) in the protein mantle of the ESM fibres influentially adsorb Cd<sup>2+</sup> cations from the precursor medium by electrostatic interactions. The amorphous Cd-ESM networks are therefore formed, and comparatively higher labile groups such as hydroxide, sulphide ions are triggered to undergo for the chemical reaction with the Cd-ESM fibre matrix. The ion migration and interaction process further compelled by the high energy UV light irradiation. The obtained NP subsequently ripen into well-defined nanocrystallites during the calcination treatment, which frequently causes enlargement and remove any hydroxyl group or carbonaceous materials involvement during the reaction.

Interestingly, the NPs do not undergo agglomeration even after calcination. This is probably due to the ESM acts here as a structure-directing or templating agent, that can restrict the hierarchical growth of the morphology and thus eliminated agglomeration. The overall synthesis process has been schematically represented in Fig. S1, SI.

## Results and discussion

### Structural and optical analysis of ESM assisted CdS

The crystallite phase of CdS determines its optoelectronic properties. Therefore, in order to understand the phase purity of the CdS, the sample obtained after annealing was characterized by XRD study, as shown in Fig. 1. All the peaks have been well indexed and matched with the hexagonal phase of CdS corresponding to the JCPDS card number 02-0549 [37]. The broadness, as well as the intense peak of the XRD, indicates the finer particle size of the CdS. The mean size of the crystallites has been calculated to be ~5 nm using the Scherrer equation.

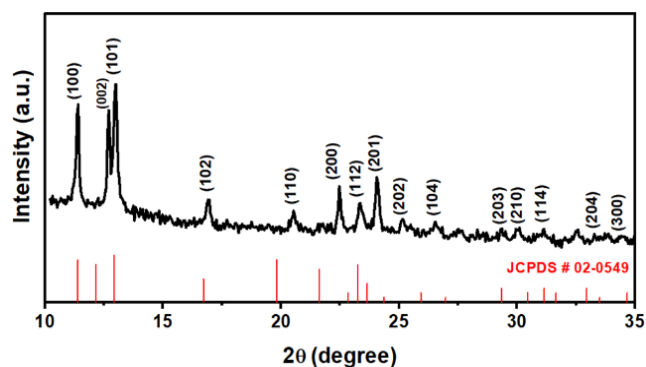


Fig. 1. XRD pattern of the ESM derived CdS powder.

The natural ESM was amorphous to X-rays, whereas the synthesized CdS exhibits high crystallinity, as evident from the XRD patterns shown in Fig. S2, SI. Ostwald ripening, in the presence of constant UV irradiation can explain this phenomenon. It has been observed that after 2 hours, many small crystals formed initially slowly disappear, except for a few that grow larger, at the expense of the small crystals, where the smaller crystals act as fuel for the growth of bigger crystals [38]. Further UV irradiation (> 2 hours), the CdS formation only resulted in enhanced crystallinity but along with the emergence of many other unidentified phases (Fig. S2, SI). Therefore, due to consideration of phase purity, 2 hours irradiation has been optimized to form the hexagonal CdS, and selected for further studies.

The UV-Vis absorption spectrum of CdS NPs exhibited an absorption edge ( $\lambda_c$ ) at ~490 nm (Fig. 2(a)), which further depicted an average particle size of 5.29 nm as derived from the Henglein's empirical formula as mentioned in equation (1), [15]

$$R(\text{CdS}) = \frac{0.1}{(0.1338 - 0.0002345 \cdot \lambda_e)} \quad (1)$$

where, R and  $\lambda_c$  denote for the diameter of the CdS particle and absorption edge (nm) recorded from UV-Vis absorption spectroscopy. The corresponding optical band gap ( $E_g$ ) was calculated ~2.5 eV by using Tauc plot as shown in equation (2), [39]

$$\alpha h\nu = A (h\nu - E_g)^{1/2} \quad (2)$$

where,  $\alpha$ ,  $\nu$ , h corresponds to the absorption coefficient, frequency and Planck's constant, respectively and considering allowed direct transition for synthesized CdS.

The emission spectra of CdS NPs has been monitored at room temperature by varying the excitation wavelengths from 340 to 390 nm, as shown in Fig. 2(b). A sharp, distinct emission peak at ~470 nm (blue emission) along with other weak peak associated at ~453, 484, 496 and 543 nm were observed against all the excitation wavelengths. The maximum intensity of the emission band was at the excitation wavelength of 380 nm.

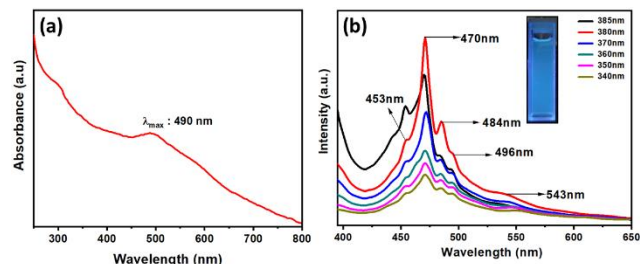


Fig. 2. (a) UV-Vis absorption spectrum and (b) excitation wavelength-dependent photoluminescence spectra of 300°C calcined CdS dispersion in water, respectively (inset shows a photograph of the CdS dispersion in water, illuminated under UV light).

The synthesized CdS sample exhibits multiple emission peaks generates from variable trap states associated with the CdS band structure. It is anticipated that the band-edge emission originated from the direct recombination of the electrons and holes from the conduction and valence band when the excitation energy is greater than the bandgap energy. In case of, defect mediated crystal structure or crystal surface existence resulted from multiple trap states between the bandgap and the emission due to the recombination of trapped electrons and holes has been exhibited in multiple emission peak generation. The ESM exhibits the emission of bright fluorescent light in the blue region of the visible spectrum. The surface compositions of ESM have been permuted with the associated  $\text{S}^{2-}$  ion and precursor  $\text{Cd}^{2+}$  ion in the presence of UV light irradiation, which results in the emission to the greenish-blue region as shown in inset of Fig. 2(b). The broadness and massive Stokes shift of the emission from  $\text{Cd}^{2+}$ -rich CdS NPs was due to the surface trap state emission [40]. It has been considered that the recombination of shallow trapped electrons and shallow trapped holes is the primary source of the surface trap state emission in the CdS NPs. The higher content of surface  $\text{Cd}^{2+}$  dangling bonds triggers in more shallow trapped electrons and shallow trapped holes, and hence the more effective surface trap state emission is associated with the band edge emission [41].

### Microstructural investigation of ESM assisted synthesized CdS Nanoparticles

Fig. 3(a) and Fig. 3(b) displays the interwoven networks of ESM fibres, which are composed of a calcified extracellular matrix and a multi-layered collagen-based membrane

consisting of organic interwoven fibre and the CdS NPs are embedded on the membrane matrix. The membrane fibres have a width ranging from nanoscale to micrometre scale and coalesce at three dimensions. As shown in **Fig. 3(b)**, the CdS are assigned particle-like morphology, which is interconnected meshwork made up of fibres ranging from 0.2 to 2  $\mu\text{m}$  in diameter. The EDX spectrum indicates about the homogeneous distribution with distinct colour contrast of elements as Cd and S from the elemental mapping diagram, as shown in **Fig. 3(c)**.

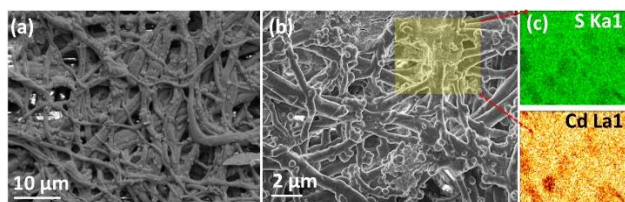


**Fig. 3.** (a), (b) SEM microstructural images of CdS nanoparticles embedded on the surface of ESM at different magnification, respectively and (c) corresponding EDX elemental analysis.

It is evident from the TEM images that the synthesized CdS formed as polycrystalline NPs and appeared as a spherical. Due to consist of three dimensional-entangled structure of highly cross-linked fibres and porous nature of ESM further influences the formation and growth of CdS. The TEM bright-field image of CdS indicates well separated distinct NP formation, as shown in **Fig. 4(a)**. Further, the average particle size was calculated of 5.2 nm, as plotted in the histogram, as shown in **Fig. 4(b)**. The obtained particle size is the quite resemblance to the calculated crystallite size from Scherer equation, and Henglein's empirical formula. The crystalline nature of the CdS NPs can be easily observed from the HRTEM image, as shown in **Fig. 4(c)**. The lattice fringes observed to each other with distances of 0.336 and 0.335 nm can be readily observed indexing to the lattice spacing of the (002) and (100) crystalline planes of hexagonal CdS crystal structure, respectively.

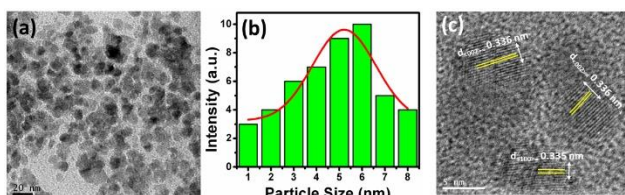


**Fig. 4.** TEM (a) bright-field image (scale: 20 nm), (b) corresponding histogram plot for particle size analysis and (c) high-resolution TEM image (scale: 5 nm) of the ESM assisted synthesized CdS nanoparticle, respectively.

### X-ray photoelectron spectroscopy studies of ESM assisted synthesized CdS Nanoparticles

XPS was performed to reveal further the chemical compositions of the ESM mediated CdS NPs, as shown in **Fig. 5**. The survey spectrum of the CdS NPs is shown in **Fig. 5(a)**. First, two characteristic peaks at  $\sim 161.3$  and  $162.4$  eV (**Fig. 5(b)**) in the bare CdS sample were attributed

to the doublet of S  $2p_{3/2}$  and S  $2p_{1/2}$ , respectively, indicating that the valence state of element S is -2. The characteristic peaks attributed to the binding energy for Cd  $3d_{5/2}$  and Cd  $3d_{3/2}$  were also observed at  $\sim 405.4$  and  $411.7$  eV, respectively, as shown in **Fig. 5(c)** [42]. The result further confirms the successful formation of CdS from the ESM mediated method.

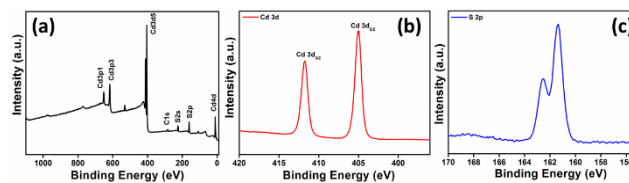


**Fig. 5.** (a) XPS survey spectrum, core level spectrum of (b) S-2p and (c) Cd-3d for the CdS nanoparticle, respectively.

### Zeta potential and Fourier-transform infrared spectroscopy analysis of ESM assisted synthesized CdS Nanoparticles

Zeta potential ( $\zeta$ ) measurements were also carried out to verify the stability of the CdS NPs in water. A zeta potential value of  $-22.5$  mV. The FTIR spectra of the CdS NPs immobilized ESM in comparison to bare ESM is shown in **Fig. S3, SI**. The infrared absorption peaks at  $\sim 3,310$ ,  $1,645$ ,  $1,432$ ,  $870$ , and  $715$   $\text{cm}^{-1}$ , which correspond to C=O, -CONH-, C-N, N-H, and C-C vibrations, respectively. This indicates the presence of peptide bonds in the ESM [43]. On the other hand, the strong bands appeared in between  $550$ - $630$   $\text{cm}^{-1}$  corresponds to the Cd-S stretching mode. Moreover, the bands assigned at  $\sim 1112$  (medium) and  $\sim 1626$  (strong)  $\text{cm}^{-1}$  are attributed to the C-S, S-H and C-O stretching modes, corresponding to the moisture adsorbed CdS NPs [18]. Medium-strong band positions  $\sim 1565$   $\text{cm}^{-1}$  and are possibly due to stretching vibrations of sulphate group. Traces of S-O peak centered at  $\sim 1076$   $\text{cm}^{-1}$  occurred in strong absorption bands. A large hump of the absorption band is observed at  $\sim 3567.66$   $\text{cm}^{-1}$  indicates labile -OH stretching due to surface adsorbed water. This hump might be due to the presence of moisture in the sample. This observation further indicates about the successful formation of CdS NPs on the surface of ESM, without disturbing its original structure.

### Mn<sup>VII</sup> ion removal using ESM assisted synthesized CdS Nanoparticles

The synthesized CdS NPs have been studied for catalytic decomposition of  $\text{KMnO}_4$  solution as an example. In details, an aqueous solution of  $0.1$  mM  $\text{KMnO}_4$  has been selected where the CdS NPs have been introduced as a catalyst for its decomposition to  $\text{MnO}_2$  and the progress of entire catalytic decomposition process has been monitored through UV-Vis spectrophotometer. The resultant analysis was also compared in the absence catalyst. In details,  $12$  mg of synthesized CdS NPs powder was introduced in  $10$  ml of  $0.1$  mM aqueous  $\text{KMnO}_4$  solution, shake it well by hand, and keep it at room temperature. The successive absorption spectra of  $\text{KMnO}_4$  decomposition were monitored

concerning time, and the results are presented in **Fig. 6(a)**. It was to be noted here that the  $\text{MnO}_4^-$  solution has given their multi characteristic absorption peaks at 505, 524, 546 and 565 nm respectively, due to metal to ligand charge transfer (MLCT) transition ( $\text{O}^{4-}\text{Mn}^{\text{VII}}$  transition) [44]. Nevertheless, after treated with CdS NPs into the  $\text{KMnO}_4$  solution, the intensity of the initial absorption peaks was started to decrease and finally, all the distinct peaks were diminished, and a new absorption peak at  $\sim 352$  nm has appeared which is indicated the characteristic peak of  $\text{MnO}_2$  [45].  $\text{MnO}_2$  NP as a degraded product, which could help to decompose other organic and inorganic pollutants in water for further study. It is due to the decomposition of  $\text{Mn}^{\text{VII}}$  (purple) to  $\text{Mn}^{\text{II}}$  (brownish yellow), and the decomposition process was completed within 50 min, which is comparatively faster than previously reported.

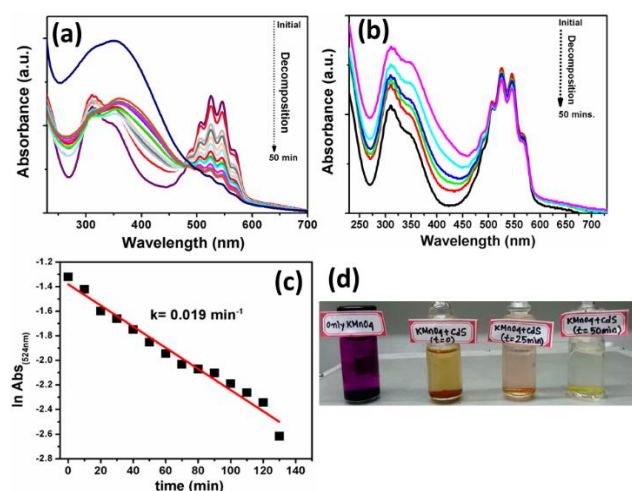


**Fig. 6.** UV-Vis absorption spectra evolutions for the catalytic decomposition of  $\text{KMnO}_4$  (a) in the presence and (b) in the absence of CdS nanoparticles, respectively, (c) shows the plot of  $\ln \text{Abs}_{524 \text{ nm}}$  vs time (min) for the above reaction and (d) the digital image of the  $\text{KMnO}_4$  decomposition reaction at various time interval towards its completion.

In case of without addition of CdS, the decomposition rate of  $\text{KMnO}_4$  solution has become less significant as shown in **Fig. 6(b)**. In this case, there was a slight decrement of higher wavelength region (501-573 nm) intensity. In contrast, there is a slight increment also of the lower wavelength peak at 310 nm, due to its auto-decomposition of a minute amount of  $\text{MnO}_4^-$  to  $\text{MnO}_4^{2-}$  ions. Thus, the catalytic adsorption nature of the synthesized CdS has shown its significant contribution towards the completion of the reaction. Also, there is a significant blue shifting of the absorption maxima as the obtained  $\text{MnO}_2$  was observed up to 50 min of the reaction in comparison to bulk  $\text{MnO}_2$  due to generation of the smaller size of  $\text{MnO}_2$ . The characteristic purple colour of the  $\text{KMnO}_4$  solution has been faded to brownish-yellow colour, and the overall reaction was completed by 50 min. **Fig. 6(c)** indicates a linear plot of  $\ln \text{Abs}_{(546 \text{ nm})}$  vs time (min) plot for the decomposition reaction follows pseudo-first-order reaction and found the rate constant ( $k$ ) value from the slope  $1.9 \times 10^{-2} \text{ min}^{-1}$ , which is comparable to the previously published reports [44,46]. The wavelength 565

nm was selected for **Fig. 6(c)** because this is one of the maxima of the reactant, where the contribution of the product's absorption is minimum. As the reaction proceeds, yellow turbidity slowly develops, and on prolonged standing, the solution turns to colourless with a brown colloidal precipitate,  $\text{Mn}^{\text{IV}}\text{O}_2$ . The failure to detect  $\text{Mn}^{\text{V}}$ , absence of an absorption maximum  $\sim 700$  nm, may be interpreted by its extreme short lifetime and undergoing a rapid disproportionation. **Fig. 6(d)** shows the digital image of the aqueous solution of the  $\text{Mn}^{\text{VII}}$  (violet) solution, which turns almost pale  $\text{Mn}^{\text{IV}}$  (brownish yellow) followed by the degraded product  $\text{MnO}_2$  at the bottom of the vial as observed after 50 min. Further, the catalytic degradation efficiency of  $\text{KMnO}_4$  solution was determined using the formula as mentioned in the **SI**, and the corresponding plot has been given in **Fig. S4, SI**. The overall reaction exhibits  $\sim 93\%$  catalytic efficiency in terms of degradation of  $\text{MnO}_4^-$  absorption peak by considering maximum absorption at 565 nm. On the other hand,  $\sim 88\%$  of  $\text{MnO}_2$  produces, as the converted product, calculated from the maximum absorption at 352 nm. Moreover, the representative TEM image of the CdS NPs after five successive cycles towards the decomposition of  $\text{KMnO}_4$  as shown inset of **Fig. S4, SI**, elucidates that the microstructure gets more agglomerated as seen after the fifth redox catalytic test. This may accountable for lesser catalytic efficiency of CdS NPs. In this study, the work function of CdS NPs is found at 2.5 eV. On the other hand, the reduction potential of  $\text{MnO}_4^-$  to  $\text{MnO}_2$  in a neutral solution is +0.595 V versus the standard hydrogen electrode (SHE). Therefore, it is expected that CdS NPs form a redox pair with the  $\text{MnO}_4^-$ , allowing the spontaneous electron transfer from CdS NPs to  $\text{Mn}^{\text{VII}}$  ions, and further may impede the MLCT process of  $\text{KMnO}_4$  to form  $\text{MnO}_2$  [47].

Besides, the distilled water itself is likely to contain reducing organic matter, which may tend to reduce  $\text{KMnO}_4$  to  $\text{MnO}_2$ , and the latter catalyzes the auto-decomposition of  $\text{MnO}_4^-$  ion [equation (3)]:



It was supposed to be expected that the initial pH should be increased towards more alkaline pH as  $\text{OH}^-$  is generated. Although, it was found that pH lies  $\sim 6.0 \pm 0.2$ . It was due to the Lewis acidic CdS (pH 4.18) having negatively charged surface sites, as observed from the zeta potential measurement, which sustains acidic medium, which favours a more suitable condition of this decomposition reaction [45,48].  $\text{MnO}_2$  is generally insoluble in acids but does react with hot concentrated hydrochloric acid to release chlorine gas. In acid solution,  $\text{H}_2\text{O}_2$  becomes a reducing agent, and the  $\text{MnO}_2$  will dissolve as like,



The reduction of  $\text{KMnO}_4$  was used to synthesized  $\alpha\text{-MnO}_2$  nanorods, one of the visible light response semiconductor photocatalysts [49]. Wang *et. al.*, (2018) reported a successful synthesis of  $\text{MnO}_2$  NP through the

ESM template route [50]. The obtained  $\text{MnO}_2$  NPs were further applied to tetracycline hydrochloride decontamination, in which nanomaterials could be separated easily by simply taking out of solutions. It has been noticed that  $\text{KMnO}_4$  modification with  $\text{MnO}_2$  ( $\text{MnO}_x$ ) shell can be comprising passages for the slow release of  $\text{MnO}_4^-$  in aquatic systems [51]. The  $\text{MnO}_2$  NPs can simultaneously help in decomposing other water pollutants like  $\text{H}_2\text{O}_2$ , organic dyes, phenol, acetic acid, sulfosalicylic acid and so on [52-54]. However, the exact mechanism associated with the effect of metal ion catalysts for permanganate degradation is still under debated. However, there have been many reports, which interpreted specific effects of metal cations in terms of bridging that facilitates electron transfer in redox systems or formation of a complex [55,56].

Most notably, the synthesized CdS can be separated easily from the ESM by complete natural drying it out, which avoided complex operation like centrifugation or filtration, making it an advantage in nanomaterial-based wastewater decontamination. The overall synthesis of ESM assisted CdS NPs along with its plausible redox coupling mechanism for  $\text{MnO}_4^-$  degradation has been schematically depicted in Fig. 7.



Fig. 7. Schematic illustration of the overall work.

## Conclusion

A new method of synthesis approach based on eggshell membrane (ESM) assisted method has been endeavoured in order to synthesize well-defined CdS nanoparticles (NPs) without employing any onerous reaction condition. The formation mechanism has been secured by the ultraviolet light assisted soakage method. The hexagonal phase formation of the synthesized CdS NPs have been further investigated by employing various physicochemical characterizations. The average particle size of ~5 nm is obtained for the synthesized NPs as investigated by the transmission electron microscopy study. Besides, excitation wavelength dependent multiple solid-state emission spectra of the NPs have been observed that resulting stokes shift of the emission due to the existence of various surface trap state of the CdS band structure. Further, the X-ray photoelectron spectroscopy study reveals about the  $\text{Cd}^{2+}$  and  $\text{S}^{2-}$  states of the synthesized nanoparticles (NPs). All these results strongly support a successful

formation of CdS NP by this “greener” method. The potentiality of the obtained NP as a catalyst has been further studied for the catalytic decomposition of aqueous  $\text{KMnO}_4$  solution as an example. The NPs exhibit an excellent catalytic activity in the reduction of toxic  $\text{Mn}^{\text{VII}}$  ion to non-toxic  $\text{Mn}^{\text{IV}}$  ion in aqueous medium at room temperature. Besides, it can generate  $\text{MnO}_2$  as the degraded product, which could help to decompose other organic and inorganic pollutants in water for its further application. The ESM assisted light-soakage synthesis technique envisages as an effective and low-cost fabrication process for sulphur based nanostructured materials. In addition, experimental results develop a cost-effective and straightforward synthesis process, which can implement as a promising tool for wastewater treatment developments for futuristic application (waste for the waste treatment).

## Acknowledgements

S.V. acknowledges the College of Engineering, Mathematics, and Physical Sciences, the University of Exeter for her PhD fellowship.

## Conflicts of interest

The authors declare no conflict of interest.

## Keywords

ESM, CdS, UV-Light, wastewater, metal-ion

Received: 02 September 2020

Revised: 20 October 2020

Accepted: 27 November 2020

## References

- Boles, M. A.; Engel, M.; Talapin, D.V.; *Chem. Rev.*, **2016**, *116*, 11220.
- Lesnyak, V.; Yarema, M.; Miao, S.; *Front. Chem.*, **2019**, *7*, 684.
- Jeevanandam, J.; Barhoum, A.; Chan, Y.S.; Dufresne, A.; Danquah, M.K.; *Beilstein J. Nanotechnol.*, **2018**, *9*, 1050.
- Ealias, A.M.; Saravanakumar, M. P.; *Mater. Sci. Engg.*, **2017**, *263*, 032019.
- Talapin, D. V.; Shevchenko, E.V.; *Chem. Rev.*, **2016**, *116*, 10343.
- Khan, I.; Saeed, K.; Khan, I.; *Arabian J. Chem.*, **2019**, *12*, 908.
- Thomas, A.; Goettmann, F.; Antonietti, M.; *Chem. Mater.*, **2008**, *20*, 738.
- Xie, Y.; Kocaeefe, D.; Chen, C.; Kocaeefe, Y.; *J. Nanomater.*, **2016**, 2302595.
- Petty, J.T.; Zheng, J.; Hud, N.V.; Dickson, R.M.; *J. Am. Chem. Soc.*, **2004**, *126*, 5207.
- McCaffrey, R.; Long, H.; Jin, Y.; Sanders, A.; Park, W.; Zhang, W.; *J. Am. Chem. Soc.*, **2014**, *136*, 1782.
- Liu, C. L.; Wu, H.T.; Hsiao, Y.H.; Lai, C.W.; Shih, C.W. et al.; *Angew. Chem., Int. Ed.*, **2011**, *50*, 7056.
- Esumi, K.; Suzuki, A.; Yamahira, A.; Torigoe, K.; *Langmuir*, **2000**, *16*, 2604.
- Das, P.P.; Samanta, S.; Blom, D.A.; Pramanik, S.; Devi, P.S.; Vogt, T.; Lee, Y.; *Nanoscale*, **2020**, *12*, 17462.
- Pramanik, S.; Chatterjee, S.; Kumar, G.S.; Devi, P.S.; *Phys. Chem. Chem. Phys.*, **2018**, *20*, 20476.
- Selvakumari, J.C.; Nishanthi, S.T.; Dhanalakshmi, J.; Ahila, M.; Padiyan, D.P.; *Appl. Surface Sci.*, **2018**, *441*, 530.
- Carvalho, J.; Araujo, J.; Castro, F.; *Waste Biomass Valor.*, **2011**, *2*, 157.
- Arias, J.L.; Fernandez, M.S.; Dennis, J.E.; Caplan, A.I.; *Tissue Res.*, **1991**, *26*, 37.
- Roy, A.; Das, P.P.; Tathavadekar, M.; Das, S.; Devi, P.S.; *Beilstein J. Nanotechnol.*, **2017**, *8*, 210.
- Pramanik, S.; Saha, A.; Devi, P.S.; *RSC Adv.*, **2015**, *5*, 33946.

20. Devi, P.S.; Banerjee, S.; Chowdhury, S.R.; Kumar, G.S.; *RSC Adv.*, **2012**, *2*, 11578.
21. Balaz, M.; *Acta Biomater.*, **2014**, *10*, 3827.
22. Su, H.; Song, F.; Dong, Q.; Li, T.; Zhang, X.; Zhang, D.; *Appl. Phys. A.*, **2011**, *104*, 269.
23. Roy, A.; Velusamy, S.; Mallick, T.K.; Sundaram, S.; *Mat. Lett.*, **2020**, *270*, 127734.
24. Murali, G.; Reddy, D.A.; Sambasivam, S.; Vijayalakshmi, R.P.; Reddy, V.R.; *Mater. Chem. Phys.*, **2014**, *146*, 399.
25. Cheng, L.; Xiang, Q.; Liao, Y.; Zhang, H.; *Energy Environ. Sci.*, **2018**, *11*, 1362.
26. Xiao, J.; Wen, B.; Melnik, R.; Kawazoe, Y.; Zhang, X.; *Phys. Chem. Chem. Phys.*, **2014**, *16*, 14899.
27. Horst, W.J.; Marschner, H.; *Plant Soil.*, **1978**, *50*, 287.
28. College of Tropical Agriculture and Human Resources (CTAHR), Managing Soil Manganese Toxicity, CTAHR, University of Hawaii at Manoa, Hawaii, USA, **1998**.
29. Sheng, Z.J.; China Manganese Indust., **2007**, *1*, 6.
30. Acharya, C.; Kar, R.N.; Sukla, L.B.; *Miner. Eng.*, **2003**, *16*, 1027.
31. Ahmed, K.A.M.; *J. Taibah Uni. Sci.*, **2016**, *10*, 412.
32. Omoike, A.I.; Harmon, D.; *Chemosphere*, **2019**, *223*, 391.
33. Chiam, S.; Pung, S.; Yeoh, F.; *Environ. Sci. Pollut. Res.*, **2020**, *27*, 5759.
34. Zhu, L.; Chen, Y.; Wu, Y.; Li, X.; Tang, H.; *Anal. Chim. Acta*, **2006**, *571*, 242.
35. Gour, A.; Jain, N.K.; *Artif. Cells Nanomed. Biotechnol.*, **2019**, *47*, 844.
36. Duan, H.; Wang, D.; Li, Y.; *Chem. Soc. Rev.*, **2015**, *44*, 5778.
37. Giribabu, G.; Murali, G.; Reddy, D.A.; Vijayalakshmi, R.P.; Rao, N.M.; *J. Nano Elec. Phys.*, **2012**, *4*, 04028.
38. Yu, Z.; Yin, B.; Qu, F.; Wu, X.; *Chem. Eng. J.*, **2014**, *258*, 203.
39. Senthilarasu, S.; Velumani, S.; Sathyamoorthy, R.; Subbarayan, A. et al.; *Appl. Phys. A.*, **2003**, *77*, 383.
40. Karan, S.; Majumder, M.; Mallik, B.; *Photochem. Photobiol. Sci.*, **2012**, *11*, 1220.
41. Wu, X.C.; Bittner, A.M.; Kern, K.; *J. Phys. Chem. B*, **2005**, *109*, 230.
42. Zhai, C.; Zhu, M.; Pang, F.; Bin, D.; Lu, C. et al.; *ACS Appl. Mater. Interfaces*, **2016**, *8*, 5972.
43. Xin, Y.; Li, C.; Liu, J.; Liu, J.; Liu, Y.; He, W.; Gao, Y.; *R. Soc. Open Sci.*, **2018**, *5*, 80532.
44. Dandapat, A.; De, G.; *J. Mater. Chem.*, **2010**, *20*, 3890.
45. Hwang, C.C.; Mou, C.Y.; *Appl. Catal. A-Gen.*, **2009**, *365*, 173.
46. Kundu, S.; Nithiyantham, U.; *Ind. Eng. Chem. Res.*, **2014**, *53*, 13667.
47. Wang, Y.; Cai, L.; Wang, Q.; Zhao, M.; Dong, L.; Xu, K.; Li, J. *Analyst*, **2020**, *145*, 836.
48. Nishimura, N.; Tanikawa, J.; Fujii, M.; Kawahara, T. et al.; *Chem. Commun.*, **2008**, 3564.
49. Wang, X.; Li, Y.; *Chem. Eur. J.*, **2003**, *9*, 300.
50. Wang, Q.; Ma, C.; Tang, J.; Zhang, C.; Ma, L.; *Nanoscale Res. Lett.*, **2018**, *13*, 1.
51. Kao, C.M.; Huang, K.D.; Wang, J.Y.; Chen, T.Y.; Chien, H.Y.; *J. Hazard. Mater.*, **2008**, *153*, 919.
52. Chiam, S.L.; Pung, S.Y.; Yeoh, F.Y.; *Environ. Sci. Pollut. Res.*, **2020**, *27*, 57595778.
53. Hu, E.; Pan, S.; Zhang, W.; Zhao, X.; Liao, B.; He, F.; *Environ. Sci. Pro. Impacts*, **2019**, *21*, 2118.
54. Chen, J.; Chen, X.; Xu, Z.; Xu, W.J. et al.; *Chem. Select*, **2016**, *1*, 4052.
55. Taube, H.; Myers, H.; *J. Am. Chem. Soc.*, **1954**, *76*, 2103.
56. Sheppard, J.C.; Wahl, A.C.; *J. Am. Chem. Soc.*, **1957**, *79*, 1020.

### Authors biography



**Anurag Roy** is a postdoctoral researcher in the Environment & Sustainability Institute, University of Exeter, Penryn campus, U.K. He is one of the leading young researchers at the material science interface between chemistry and physics aspects and recognized as such in the community. He is a fellow of Indian Chemical Society. Also, he has awarded with INSPIRE PhD fellowship (Govt. of India), Newton-Bhabha PhD placement program, JUICE (India-UK) Overseas placement and GW4 Climate symposia.



**Sasireka Velusamy** is a PhD student of the College of Engineering, Mathematics, and Physical Sciences, University of Exeter, Penryn Campus, U.K. Her research topic is related to the metal oxide nanoparticle embedded graphene oxide membrane fabrication for industrial wastewater treatment.



**Prof. Tapas K. Mallick** is a Professor and Chair in Clean Technologies, Renewable Energy and Lead of Solar Energy Research Group within the Environment & Sustainability Institute. He is also Director and Scientific Advisor of the BuildSolar Limited. He is an author and co-author of more than 300 papers (6k+ citation). He is actively involved in various European and Industrial funded research projects in the area of Solar Energy.



**Dr Senthilarasu Sundaram** is a Senior Lecturer in Renewable Energy, University of Penryn Campus, U.K. His research focus is on third-generation Photovoltaics involving different technologies, as well as on the applications of nanostructured oxide materials and developing flexible solar cells on metal and polymer foils. He is an author and co-author of more than 150 papers (3k+ citation).

### Graphical abstract

An effort to synthesize CdS nanoparticles (NPs) through a domestic waste, eggshell membrane (ESM) on UV light irradiation; this is a unique synthesis approach compared to others traditional synthesis methods. In addition, to study the effectivity of CdS NPs as an excellent catalyst for Mn<sup>VII</sup> ion degradation, which converts to Mn<sup>II</sup> by 50 min. Our results show relatively faster removal kinetics compared to other available reports.

